American Mineralogist, Volume 75, pages 1327–1341, 1990

Experimental investigation of andradite and hedenbergite equilibria employing the hydrogen sensor technique, with revised estimates of $\Delta_f G^0_{m,298}$ for andradite and hedenbergite

DAVID P. MOECHER
Department of Earth and Space Sciences, State University of New York, Stony Brook, New York 11794-2100, U.S.A.
I-MING CHOU
959 National Center, U.S. Geological Survey, Reston, Virginia 22092, U.S.A.

ABSTRACT

Hydrothermal experiments were carried out at 2 kbar, 600–860 °C to resolve discrepancies among previous studies on f_{O_2}-T stability relations for the following equilibria: (1) andradite (And) = hematite (Hm) + wollastonite (Wo), (2) And = magnetite (Mt) + Wo + O_2, (3) And + quartz (Qz) = hedenbergite (Hd) + Wo + O_2, and (4) And + Mt + Qz = Hd + O_2. A variety of O buffer and H_2 generation techniques were used to access a wide range of f_{O_2}-T conditions: (1) the conventional solid O buffer technique, (2) the addition of CO_2 or NaCl to the conventional assemblage f_{O_2} buffer + H_2O, and (3) mixtures of Ar and H_2O in the pressure vessel, with f_{O_2} buffered by the pressure vessel wall. These techniques allow isobaric reversal of equilibria dependent on f_{O_2} and temperature to be demonstrated by an f_{O_2} bracket at a constant temperature rather than in a temperature bracket along an O buffer. The f_{O_2} for each experiment was monitored by a f_{H_2} sensor.

Crystalline starting materials were 97–100% of end-member composition, as determined by electron microprobe and X-ray diffraction. No experimental product deviated by more than 3% from the starting composition. The effect of solid solution in the products is to shift the position of a reversal by no more than 0.1 log unit in f_{O_2}.

The results yielded an internally consistent set of experiments on andradite and hedenbergite stability. The $\Delta_f G^0_{m,298}$ for andradite and hedenbergite calculated from the data are -5428.0 ± 5.9 and -2676.6 ± 5.3 kJ/mol, respectively.

INTRODUCTION

Metamorphic equilibria involving andradite and hedenbergite have numerous applications in a wide variety of metamorphic settings. Most studies have dealt with the determination of the oxygen fugacity and temperature (f_{O_2}-T) attending formation of Fe-rich skarns, in which andradite-rich garnet and (or) hedenbergite-rich clinopyroxene assemblages are associated with deposits of Fe, Cu, Zn, Pb, W, Mo, or Sn ores (e.g., Einaudi et al., 1981; Meinert, 1982). Andradite-rich garnet solid solutions occur in calcareous gneisses and skarns, and are useful in constraining fluid composition by 24 quartz + 24 calcite + 2 hematite + 4 magnetite + O_2 = 8 andradite + 3 CO_2 (Taylor and Liou, 1978). Hedenbergite is important in temperature-dependent equilibria such as the exchange of Fe and Mg between coexisting garnet and clinopyroxene (Ellis and Green, 1979; Pattison and Newton, 1989), and in pressure-dependent equilibria such as 3 hedenbergite + 3 anorthite = 2 grossular + almandine + 3 quartz (Moecher et al., 1988). The equilibrium 3 titanite + 2 magnetite + 3 quartz = 3 hedenbergite + 3 ilmenite + O_2 has been used to constrain f_{O_2} during crystallization of granitic plutons (Wones, 1989). The andradite component in garnets from mantle peridotites has been used to calculate f_{O_2} in the upper mantle by equilibria such as 2 andradite + 6 enstatite + 4 ferrosilite = 6 diopside + 4 fayalite + O_2 (Luth et al., 1989). Accurate free-energy data for andradite and hedenbergite are necessary for all of these applications, and an internally consistent set of experimental phase equilibria is a critical component in constraining these data.

Previous experimental studies have produced sufficient data to outline with reasonable precision the f_{O_2}-T stability fields and phase relations of andradite and hedenbergite (Huckenholz and Yoder, 1971; Gustafson, 1974; Liou, 1974; Suwa et al., 1976; Burton et al., 1982). However, Moecher et al. (1988) demonstrated discrepancies among the above experimental studies on the stability of andradite and hedenbergite. Moecher et al. (1988) could not simultaneously fit the experimental constraints on the equilibria

$$\text{And} = \text{Hm} + 3\ \text{Wo} \quad (1)$$

(Huckenholz & Yoder, 1971; Suwa et al., 1976);

$$6\ \text{And} = 4\ \text{Mt} + 18\ \text{Wo} + O_2 \quad (2)$$

(Gustafson, 1974);

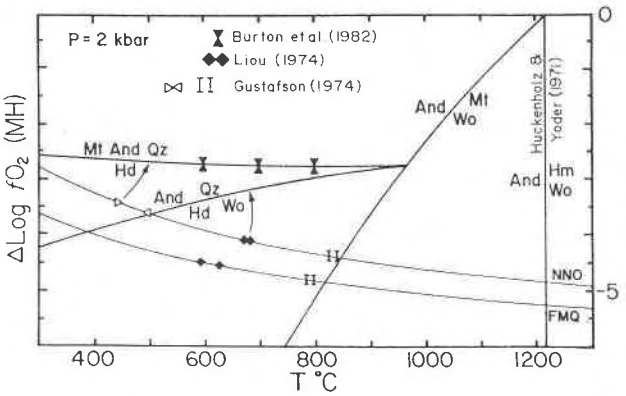

Fig. 1. Equilibria from previous experimental work at 2-kbar pressure [relative to magnetite-hematite (MH) buffer] relevant to the present study (from Moecher et al., 1988). The positions of the equilibria were calculated assuming they fit the results of Huckenholz and Yoder (1971) on And = Hm + Wo, the MH buffer calculated from the data of Robinson et al. (1982), and the results of Burton et al. (1982) on And + Mt + Qz = Hd + O_2. The calculated positions of And = Mt + Wo + O_2, And + Qz = Hd + Wo + O_2, and And + Mt + Qz = Hd + O_2 do not agree with reversals of Liou (1974) and Gustafson (1974) for the Ni-NiO (NNO) and fayalite-magnetite-quartz (FMQ) buffers (calculated positions of latter two reactions and corresponding reversals shown by arrows).

$$2\ \text{And} + 4\ \text{Qz} = 4\ \text{Hd} + 2\ \text{Wo} + \text{O}_2 \qquad (3)$$

(Liou, 1974); and

$$3\ \text{And} + \text{Mt} + 9\ \text{Qz} = 9\ \text{Hd} + 2\ \text{O}_2 \qquad (4)$$

(Gustafson, 1974; Burton et al., 1982), as shown in Figure 1. The discrepancies among the experimental data preclude accurate determination of the free energies of andradite and hedenbergite.

This study is an attempt to resolve the discrepancies in the experimental data base on the f_{O_2}-T stability of andradite and hedenbergite. Hydrothermal experiments were carried out on Equilibria 2 through 4 at 2-kbar fluid pressure and between 600 and 860 °C. From these experimental data and published heat capacity and volume data for the appropriate phases, we calculated revised values of the molar Gibbs free energy ($\Delta_f G^0_{m,298}$) for andradite and hedenbergite.

Experimental methods

Apparatus

Hydrothermal experiments were carried out in cold-seal pressure vessels of Stellite 25[1] that were 30.5 cm long × 3.2 cm (od) × 0.6 cm (id), with stainless steel filler rods. Graphite filler rods were used for experiments employing the graphite-methane (CCH_4) buffer. Horizontal, Pt-wound furnaces were used, with power maintained by solid-state temperature controllers. For most experiments Ar was used as the pressure medium; for some, mixtures of Ar and H_2O were used. All experiments were carried out at a pressure of 2 kbar. Pressure was measured with a Heise pressure gauge that employs a standard bourdon tube. The gauge was compared with three other Heise gauges, one of which was calibrated in the factory. Pressure (accurate to ±50 bars) was monitored daily and did not fluctuate from 2 kbar by more than 1%.

Temperature was measured with sheathed chromel-alumel thermocouples inserted in wells drilled into the base of the pressure vessel and parallel to the vessel bore. For each furnace, external thermocouples were calibrated by using a pressure vessel equipped with an internal thermocouple assembly. The purpose of the assembly was to characterize the thermal environment of a sample 2.54 cm long in a pressure vessel with filler rods. The internal assembly consisted of (1) a triple-junction type chromel-alumel thermocouple with the three junctions spaced 1.27 cm apart on the tip of the thermocouple (this thermocouple was calibrated against the melting points of Sn, Zn, and Al), (2) stainless steel filler rods, drilled to allow passage of the thermocouple, and (3) an Au capsule 2.54 cm long fitted onto the tip of the thermocouple. The assembly was sealed within a pressure vessel having the same specifications as the vessels to be used in the experiment. For each furnace, temperature gradients in the immediate vicinity of the sample were determined using this assembly. The temperature difference between the external and internal thermocouples (0 to +3 °C, depending on the furnace and temperature of the experiment) was recorded and used to determine temperatures of the experiments. The assembly also allowed determination of the position in the furnace that produced the smallest gradient in temperature among the three internal thermocouple junctions. Temperature differences along the internal assembly were at most 3 °C, and the majority were ≤2 °C. Temperatures reported for each experiment were judged accurate to ±5 °C. Calibrations were made for each furnace at the start and completion of the study, using different calibration assemblies. Temperature differences for the two calibrations were well within the quoted accuracy of ±5 °C.

Samples were quenched in a stream of compressed air until the vessels were cool enough to place in an H_2O bath without the H_2O vaporizing. Using the internal thermocouple assembly described above, it was determined that the time needed to quench from 600–800 °C to room temperature ranged from 2–4 min.

Starting materials

Synthetic and natural crystalline phases were used as starting materials. All phases were characterized using the optical microscope, the X-ray diffractometer (XRD), the scanning electron microscope (SEM), and the electron microprobe. Wavelength dispersive microprobe analyses were performed on the automated ARL-SEMQ instrument at the U.S. Geological Survey, Reston, Virginia. Operating conditions were 15 kV, 0.1 μA beam current,

[1] Any use of trade names in this report is for descriptive purposes only and does not constitute endorsement by the U.S. Geological Survey.

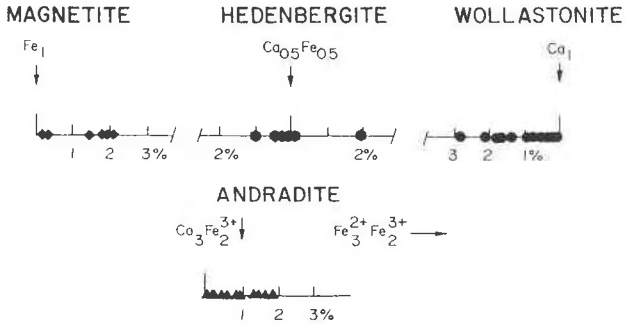

Fig. 2. Extent of predominant solid solutions in experimental starting materials and products. Starting material compositions denoted by arrows. For magnetite, hedenbergite, and wollastonite products, the predominant solid solution is Ca-Fe^{2+} (at.%). For andradite starting material and products, the predominant solid solution is $Ca_3Fe_2^{3+}$-$Fe_3Fe_2^{3+}$, with approximately 1 mol% hydroandradite component (not shown).

20 s counting times, and a focused (1-μm) beam. The X-ray correction procedure was based on the method of Bence and Albee (1968) using the α-factors of Albee and Ray (1970). For the silicates, natural hedenbergite, natural wollastonite, and synthetic acmite were used as standards for Si, Ca, and Fe, respectively. For magnetite, a natural magnetite was used as an Fe standard. Unit-cell refinements were carried out on data calculated from automated powder diffractometer scans made at 0.25° 2θ/min using Ni-filtered Cu$K\alpha$ radiation, with BaF_2 as an internal standard (Huebner and Papike, 1970). The chemical compositions and lattice parameters of starting materials are listed in Table 1. The starting materials employed in this study were 97–100% of end-member composition (Table 1, Fig. 2). The effects of solid solutions on displacement of end-member equilibria are discussed later.

The natural phases used for starting materials were wollastonite from Lewis, New York, and Brazil quartz. SEM and microprobe investigation of a thin section of the wollastonite revealed the presence of trace quantities of 10 μm-sized inclusions of diopside, calcite, and quartz. The quantity of these inclusions was estimated to be much less than 1 vol%. The unit-cell parameters for wollastonite (Table 1) agree with previous studies (Buerger and Prewitt, 1961; Matsueda, 1973; Krupka et al., 1985). Microprobe analysis indicated virtually pure wollastonite (Table 1, Fig. 2).

Andradite was synthesized in Au capsules from gels of

TABLE 1. Chemical composition and crystallographic parameters of starting materials

	Andradite				
	I*	II*	Hedenbergite	Wollastonite	Magnetite
SiO_2	34.92(52)	35.75(59)	48.15(70)	51.51(6)	0.22(8)
TiO_2	na	na	na	0.00	na
Al_2O_3	na	na	na	0.08(1)	0.00
FeO**	29.16(99)	27.91(30)	29.06(41)	0.02(3)	93.04(72)
Fe_2O_3	32.43	31.01	—	—	68.66
MnO	na	na	na	0.01(0)	na
MgO	na	na	na	0.40(2)	0.03(1)
CaO	32.65(50)	33.18(23)	22.50(63)	47.35(27)	0.00
Na_2O	na	na	na	0.01(2)	na
FeO†	—	—	—	—	31.30
Sum	100.00	99.94	99.71	99.38	100.21
N	13	10	5	10	22
Cations	8	8	4	2	3
Si	2.962	3.022	1.999	1.000	0.008
Ti	—	—	—	0.000	—
Al	—	—	—	0.002	0.000
Fe^{3+}	2.000	1.973	—	—	1.984
Fe^{2+}	0.071	—	1.001	0.001	1.006
Mn	—	—	—	0.000	0.000
Mg	—	—	—	0.012	0.002
Ca	2.967	3.005	1.000	0.985	0.000
Na	—	—	—	0.001	—
X_{Em}‡	0.97	0.99	1.00	0.99	0.99
a Å	12.058(1)	12.064(1)	9.845(1)	7.929(1)	8.394(3)
b Å	12.058(1)	12.064(1)	9.028(2)	7.321(2)	8.394(3)
c Å	12.058(1)	12.064(1)	5.249(1)	7.069(1)	8.394(3)
α	90.00	90.00	90.00	89.95(3)	90.00
β	90.00	90.00	104.81(2)	95.25(2)	90.00
γ	90.00	90.00	90.00	103.42(2)	90.00
V Å^3	1753.3(2)	1756.0(0)	451.0(1)	397.4(1)	591.4(6)
N	12	14	20	22	6

Note: na: not analyzed. Numbers in parentheses are 1σ standard deviations for the average of microprobe analysis of N grains, and standard errors for unit-cell refinements based on N reflections.

* Andradite I and II synthesized from gels using metallic iron and ferric nitrate, respectively, as the source of Fe.

** Fe calculated as FeO from microprobe data, recalculated as Fe_2O_3 for andradite, and calculated as Fe_2O_3 and FeO for magnetite, based on stoichiometry.

† FeO recalculated from stoichiometry.

‡ Mole fraction of end-member component.

appropriate composition at 700–725 °C and 2 kbar of Ar pressure. Tetraethyl orthosilicate was used as the source of Si, calcite as the source of Ca, and either metallic Fe (andradite I, Table 1) or ferric nitrate (andradite II) as the source of Fe. Optical and SEM inspection, XRD scans, and energy-dispersive analysis indicated the presence of wollastonite (approximately 5 vol%) in batches of both types of synthetic andradite and traces of what is probably larnite in batches of andradite II. The synthetic andradite crystals ranged in size from 1 to 10 μm, with most in the range 2–6 μm. In immersion oil, andradite I was brownish red in color, whereas andradite II was greenish yellow in color. Microprobe analyses of both andradites are within a 2σ uncertainty of an ideal andradite analysis. The unit-cell parameter for andradite I [12.058(1) Å] agrees with the value for andradite of Huckenholz and Yoder (1971) and Huckenholz and Fehr (1982).

Hedenbergite was produced by conversion of ferrobustamite in Ag25-Pd75 capsules at 700 °C and 2 kbar, with methane as the pressure medium. The ferrobustamite (supplied by H. T. Haselton, U.S. Geological Survey) was synthesized from glass of appropriate composition in a piston-cylinder apparatus (Haselton et al., 1987). The hedenbergite was pale greenish gray, and crystals ranged in size from 1 to 8 μm. No other phase was observed by optical and SEM inspection or on XRD scans. Microprobe analysis indicated end-member hedenbergite (Table 1, Fig. 2), and refined unit-cell parameters agree with previous studies (Lindsley, 1967; Veblen and Burnham, 1970; Cameron et al., 1973; Kandelin and Weidner, 1988).

Magnetite was recrystallized hydrothermally from reagent-grade magnetite with NH_4Cl solution at 300 °C in a Morey vessel (supplied by J. L. Haas, Jr., U.S. Geological Survey). Microprobe analysis indicated trace quantities of Si and Mg. No other phases were present, except hematite as rare lamellar exsolutions in magnetite. The unit-cell parameter agrees reasonably well with other studies.

Experimental products and criteria for reaction direction

Experimental products were examined by optical microscopy, XRD, SEM, and microprobe techniques. Most of the silicate charge (totaling 30–40 mg of powder) was scanned on an X-ray diffractometer; 1–2 mg were set aside for SEM and microprobe analysis. Reaction direction was inferred from the comparison of the proportion of phases in starting materials and products, as determined by microscopic examination, and from relative changes in peak intensities on XRD scans. In most cases, this system yielded an unambiguous indication of reaction. SEM studies were carried out to evaluate the utility of using mineral textures as indicators of reaction direction. However, no systematic pattern of growth or dissolution features could be discerned.

Wollastonite is known to incorporate Fe at high temperatures (e.g., Rutstein, 1971), the Fe^{3+}/Fe^{2+} ratio of andradite is dependent on f_{O_2} (e.g., Gustafson, 1974), and magnetite may contain significant Si or Ca. Therefore, microprobe analyses were made on as many of the phases in the sample as was practical (andradite, hedenbergite, wollastonite, or magnetite), or on phases in the assemblage that grew at a particular f_{O_2} and T. Analyses are listed in Table 2 and may be compared in Figure 2. Analyses in Table 2 are averages of a minimum of 3 grains per phase. Unit-cell refinements were also carried out on andradite in the products for Equilibrium 2.

The f_{O_2} buffer and H_2 sensor techniques

The conventional method for locating equilibria such as 2, 3, and 4 in f_{O_2}-T space is based on the O and H_2 buffer technique of Eugster (1957), the practical aspects of which have been reviewed by Huebner (1971). The standard capsule configuration consists of the O buffer [e.g., Ni-NiO (NNO)] and H_2O, enclosing a Pt (or Ag-Pd alloy) capsule containing the silicate sample and H_2O, all contained within a welded Au capsule. The O buffer and H_2O generate an equilibrium f_{H_2} that is imposed on the enclosed sample by diffusion of H_2 through the Pt and into the sample. If the f_{H_2O} within the sample and in the external buffer are equal, the f_{O_2} of both subsystems is also the same. The position of an f_{O_2}-dependent equilibrium is constrained by varying temperature and shifting along a buffer until one encounters a change in the stable assemblage (e.g., Gustafson, 1974; Liou, 1974). This technique is adequate for Equilibrium 2, whose steep slope relative to NNO, Co-CoO (CCO), or CCH_4 buffer curves results in a series of intersections within a limited temperature interval (Fig. 3). The position of Equilibrium 2 can be precisely constrained by reversing the reaction along the NNO, CCO, and CCH_4 buffers. However, Equilibria 3 and 4 exhibit shallower slopes in log f_{O_2}-T space that intersect at a lower angle or are nearly parallel to the conventional O buffers. This geometry makes it more difficult to obtain intersections along any two buffers. Furthermore, Equilibrium 4 lies in a region of f_{O_2}-T space where there is no calibrated buffer above 600 °C.

An alternative approach for reversing f_{O_2}-dependent equilibria was attempted by Burton et al. (1982), who applied the H_2 sensor method of Chou and Eugster (1976). The latter method is based on the Ag-AgCl buffer,

$$Ag + HCl = AgCl + 1/2H_2, \quad (5)$$

(Frantz and Eugster, 1973), which is sensitive to f_{H_2}, the equilibrium constant being

$$K_5 = [a_{AgCl} \cdot f_{H_2}^{1/2}]/[a_{Ag} \cdot f_{HCl}]. \quad (6)$$

The Ag-AgBr or Ag-AgI buffers also may be used. In practice, the sensor consists of a mixture of solid Ag and AgCl, sealed in a Pt capsule with H_2O or HCl. The sensor and charge capsules are then sealed in an Au tube with the O buffer and H_2O. The equilibrium f_{H_2} generated by the buffer + H_2O assemblage is imposed on the charge and sensor by diffusion of H_2 through the Pt capsules (Fig. 4A). Depending on whether pure H_2O or an HCl solution is included in the sensor, HCl will form or decompose in

response to the ingress or egress of H_2 into or out of the sensor. Measurement of the HCl concentration allows calculation of the equilibrium f_{H_2}, assuming K_5 is known. K_5 was calibrated against the NNO buffer as a reference, using the data of Frantz and Marshall (1984) on the dissociation of HCl. Details on the calibration and underlying assumptions of the H_2 sensor method are presented in Chou (1978, 1987a).

The utility of the H_2 sensor method is that one can investigate f_{O_2}-dependent equilibria directly, by enclosing a sensor within the silicate assemblage and allowing it to measure the equilibrium f_{H_2} (Fig. 4C). If the f_{H_2O} in the sample is known, f_{O_2} may then be calculated. Burton et al. (1982) investigated Equilibrium 4 using this technique.

In this study we employed the conventional approach of obtaining reversals along an O buffer to constrain the location of Equilibrium 2. For experiments employing the conventional technique, H_2 sensors were included in the samples to monitor f_{H_2} during long experiments. For Equilibria 3 and 4, we used a combination of the conventional approach, the method of Burton et al. (1982), and two other general approaches using H_2 sensors. Rather than shifting along a buffer by varying temperature, one can vary the f_{H_2} imposed on a silicate charge at constant temperature, and therefore can shift to higher or lower values of f_{O_2}. The variation of imposed f_{H_2} is attained in two ways:

1. Reduction in the f_{H_2O} in equilibrium with an O buffer by adding a second fluid component (Whitney, 1972; Chou, 1988). At constant f_{O_2}, reduction in f_{H_2O} results in reduced f_{H_2} in the external buffer assemblage. This approach imposes an f_{H_2} lower than the buffer system with pure H_2O. We used CO_2 generated by the addition of $Ag_2C_2O_4$ to the buffer + H_2O mixture, or mixtures of an O buffer, H_2O, and excess NaCl. The former allows variation of f_{H_2} by continually varying the ratio of CO_2 to H_2O. With excess NaCl (halite saturation), the latter defines f_{O_2}, f_{H_2}, and f_{H_2O} at a given temperature and pressure. Gunter et al. (1983) determined the liquidus temperature of halite and its corresponding halite-saturated fluid composition at pressures up to 4 kbar in the binary system NaCl-H_2O. The capsule configuration needed is identical to the conventional technique, with the addition of $Ag_2C_2O_4$ or NaCl and a H_2 sensor (Fig. 4B).

2. Variation of f_{H_2O} and f_{H_2} by using mixtures of Ar and H_2O as the pressure medium, with f_{O_2} imposed by the cold-seal vessel. The charge and sensor capsules are sealed in the vessel without the buffer-H_2O jacket (Fig. 4D). This technique is similar to the traditional Shaw technique (Shaw, 1963, 1967), and to the technique of Popp et al. (1984) who used mixtures of Ar and CH_4 to obtain a desired f_{H_2}. In our experiments, the f_{H_2} in two vessels containing pure (nominally) Ar or H_2O was measured by a H_2 sensor in each vessel. Ar produced the lower and H_2O the higher f_{H_2}. For the Ar experiments, it is likely that contamination by moisture in the vessel, hydrocarbons from pump oil, and impurities in the gas allowed generation of a finite f_{H_2}. Intermediate values of f_{H_2} were produced by empirically adjusting the partial pressures of the two gases in one experiment. The f_{H_2} was measured by a H_2 sensor included in each experiment. Reversal of a reaction was then demonstrated by monitoring the change in stable mineral assemblage as a function of f_{H_2} (and hence f_{O_2}), at constant pressure and temperature.

The calculation of f_{H_2} for a given experiment is based on measurement by coulometric titration of the equilibrium HCl concentration of the experiment. The data of Frantz and Marshall (1984) indicated that HCl is mostly associated at temperatures greater than 600 °C at 2 kbar. At 25 °C, HCl is mostly dissociated, so that $m_{(HCl)}$ at P and T may be approximated by $m_{(Cl^-)}$ at 1 atm and 25 °C. The measurement of M_{Cl^-} was performed on a Buchler chloridometer and is accurate to 0.002 M. Measured molarities of chloride (M_{Cl^-}) were converted to molality of HCl (m_{HCl}) (Chou, 1987a, p. 76). These measured values and 1σ standard deviations of the average from three or four 3 μL aliquots of fluid are included in the list of experimental data (Table 3).

The H_2 sensor technique allows measurement of f_{H_2} by Equilibrium 5. Because accurate thermodynamic data for substances involved in Equilibrium 5 are not available, the sensor must be calibrated against an O buffer by measuring the m_{HCl} produced in the reaction of AgCl with H_2 generated by that buffer. Because the relationship among f_{O_2}, f_{H_2O}, K_W, and f_{H_2} holds for both the buffer and the unknown, f_{O_2} need not be directly calculated. Rather, from the measured m_{HCl} for a sample and the reference buffer, f_{O_2} of the sample is calculated from the relation

$$f^s_{O_2P,T} = f^r_{O_2P,T} \cdot [m^r_{HCl}/m^s_{HCl}]^4 \quad (7)$$

or

$$\log f^s_{O_2P,T} = \log f^r_{O_2P,T} + 4 \log m^r_{HCl} - 4 \log m^s_{HCl} \quad (8)$$

where r refers to the reference buffer (values of f_{O_2} for NNO from Huebner (1971), and m_{HCl} from calibration experiments), s refers to values for the sample, and m_{HCl} is the measured value of molarity for standard and sample at 1 bar, 25 °C. A more detailed derivation for these relations was presented by Chou (1987a). Values of f_{O_2} calculated for experiments are listed in Table 3.

Experiments employing the CCH_4 H_2 buffer used the Ag-AgBr buffer in the H_2 sensors. The Ag-AgBr buffer yields HBr solutions that are about an order of magnitude less concentrated than the HCl solutions produced by Ag-AgCl at the same P-T-f_{H_2} conditions. The reference buffer for these experiments was the CCO buffer as calibrated by Chou (1978; revised equation in Chou, 1987a).

Sample and buffer configuration

For experiments employing the conventional buffering technique, the sample charge and a H_2 sensor were sealed with approximately 800 mg of buffer and 35 mg of distilled, deionized H_2O in Au capsules of 25 mm × 4.4 mm (od) × 4.0 mm (id), welded at both ends. For experiments employing mixtures of a buffer with $Ag_2C_2O_4$

TABLE 2. Microprobe analysis of experimental products

Wollastonite + magnetite = andradite experiments

Wollastonite

Experiment no.	6	8a	8b	9	18	19a	19b	20	20b	21	22
T (°C)	750	775	775	760	715	710	720	750	740	840	860
buffer	CCO	CCO	CCO	CCO	WO2	CH4	CH4	CH4	CH4	NNO	NNO
SiO_2	50.87	51.61	51.66	50.92	51.06	50.87	50.91	50.50	51.46	51.61	51.03
FeO	0.22	0.45	0.90	0.91	0.49	0.47	0.74	1.71	0.41	0.98	0.86
CaO	48.01	47.61	46.94	47.33	48.16	47.91	47.12	47.11	48.12	47.03	47.14
Sum	99.10	99.67	99.50	99.16	99.71	99.25	98.77	99.32	99.99	99.62	99.03
Si	0.993	1.002	1.006	0.995	0.991	0.992	0.998	0.986	0.996	1.004	0.998
Fe	0.004	0.007	0.015	0.015	0.008	0.008	0.012	0.028	0.007	0.016	0.014
Ca	1.004	0.991	0.979	0.991	1.001	1.001	0.990	0.986	0.998	0.980	0.982

Andradite

Experiment no.	1c	2c	6	8a	8b	9	19a	19b	20b	21	22
T (°C)	600	700	750	775	775	760	710	720	740	840	860
buffer	NNO	CCO	CCO	CCO	CCO	CCO	CH4	CH4	CH4	NNO	NNO
SiO_2	34.85	35.41	34.94	35.13	34.98	35.17	35.02	34.96	35.41	35.42	35.24
FeO*	29.35	29.39	29.35	29.17	30.02	29.38	29.63	29.66	29.23	29.69	28.57
Fe_2O_3	32.62	32.66	32.62	32.42	33.35	32.65	32.93	32.95	32.47	32.99	31.74
CaO	32.21	32.53	32.52	32.28	31.86	32.07	32.12	31.90	32.19	32.09	32.56
Sum	99.68	100.60	100.08	99.83	100.19	99.89	100.07	99.81	100.07	100.50	99.54
Si	2.969	2.987	2.963	2.986	2.970	2.990	2.974	2.977	3.003	2.995	2.999
Fe^{3+}	2.000	2.000	2.000	2.000	2.000	2.000	2.000	2.000	2.000	2.000	2.000
Fe^{2+}	0.092	0.074	0.082	0.074	0.131	0.089	0.105	0.112	0.073	0.099	0.033
Ca	2.940	2.939	2.955	2.940	2.898	2.921	2.922	2.911	2.925	2.906	2.968

Magnetite

Experiment no.	7a	8a	20	20b	22
T (°C)	800	775	750	740	860
buffer	CCO	CCO	CH4	CH4	NNO
SiO_2	0.23	0.12	0.66	0.38	0.22
Al_2O_3	0.00	0.00	0.16	0.09	0.00
FeO*	93.41	92.91	92.64	93.54	93.01
FeO**	31.13	30.72	31.51	31.57	30.90
Fe_2O_3	69.27	69.17	67.98	69.92	69.08
CaO	0.39	0.43	0.46	0.20	0.54
MgO	0.03	0.06	0.08	0.08	0.02
Sum	101.05	100.50	100.85	102.24	100.76
Si	0.009	0.005	0.025	0.007	0.009
Al	0.000	0.000	0.007	0.000	0.001
Fe^{3+}	1.983	1.991	1.943	1.985	1.982
Fe^{2+}	0.991	0.983	1.002	0.991	0.986
Ca	0.016	0.018	0.019	0.015	0.022
Mg	0.002	0.003	0.005	0.001	0.001

Hedenbergite-andradite-wollastonite-quartz experiments

Wollastonite

Experiment no.	1c	1e	2d	2e	4a	7b-3	9d	12a
T (°C)	650	650	665	665	700	800	600	750
buffer	NNO	NaCl	NNO	NaCl	NNO	HW	NNO	NNO
SiO_2	51.75	52.20	52.23	51.54	51.85	52.15	51.45	52.55
FeO	0.55	0.11	0.56	0.17	0.48	0.52	0.33	0.68
CaO	47.47	47.38	47.63	47.09	47.07	47.09	48.85	46.90
Sum	99.77	99.69	100.42	98.80	99.40	99.76	100.63	100.13
Si	0.987	1.013	1.007	1.009	1.010	1.012	0.989	1.017
Fe	0.009	0.002	0.009	0.003	0.008	0.008	0.005	0.011
Ca	0.987	0.985	0.984	0.988	0.982	0.979	1.006	0.972

Hedenbergite

Experiment no.	1c	2d	2e	4a	7b-3	9d	12a
T (°C)	650	665	665	700	800	600	750
buffer	NNO	NNO	NNO	NNO	HW	NNO	NNO
SiO_2	48.93	48.57	48.38	48.93	49.06	48.84	48.31
FeO	29.40	29.04	28.66	28.72	28.38	28.66	27.74
CaO	22.00	22.48	21.94	22.02	22.22	21.87	23.34
Sum	100.33	100.09	98.98	99.67	99.66	99.37	99.39
Si	2.015	2.004	2.018	2.027	2.031	2.030	2.002
Fe	1.014	1.003	1.001	0.996	0.983	0.997	0.962
Ca	0.971	0.994	0.981	0.977	0.985	0.974	1.036

TABLE 2.—*Continued*

	Andradite					
Experiment no.	1c	1e	2e	7b-3	9d	12d
T (°C)	650	650	665	800	600	750
buffer	NNO	NaCl	NaCl	HW	NNO	NaCl
SiO_2	35.23	35.87	35.32	36.26	35.68	35.60
FeO*	30.26	28.67	28.34	28.85	28.32	28.45
Fe_2O_3	33.61	31.85	31.49	32.05	31.46	31.61
CaO	31.73	32.95	32.64	31.49	32.44	32.59
Sum	100.57	100.67	99.45	99.80	99.58	99.80
Si	2.982	3.016	3.006	3.082	3.033	3.023
Fe^{3+}	2.000	2.000	2.000	2.000	2.000	2.000
Fe^{2+}	0.141	0.016	0.017	0.050	0.013	0.020
Ca	2.877	2.968	2.976	2.867	2.954	2.957

Hedenbergite = andradite + magnetite + quartz experiments

	Hedenbergite			
Experiment no.	4a	4b	6a	7e
T (°C)	600	600	650	700
buffer	NNO	NaCl	NNO	AH
SiO_2	49.02	49.00	48.86	48.86
FeO	28.66	28.63	28.56	28.72
CaO	22.23	22.07	21.94	21.92
Sum	99.91	99.70	99.36	99.50
Si	2.025	2.029	2.030	2.028
Fe	0.991	0.992	0.993	0.998
Ca	0.984	0.979	0.977	0.975

	Andradite					
Experiment no.	4b	6b	6g	7a	7e	8a
T (°C)	600	650	650	700	700	750
buffer	NaCl	VA	AH	VA	AH	VA
SiO_2	35.77	35.81	35.55	35.60	35.83	36.03
FeO*	28.39	28.32	28.56	29.25	28.23	28.08
Fe_2O_3	31.54	31.46	31.73	32.50	31.36	31.20
CaO	32.60	33.11	32.48	32.46	32.65	33.37
Sum	99.91	100.38	99.76	100.56	99.84	100.68
Si	3.030	3.017	3.018	3.003	3.036	3.026
Fe^{3+}	2.000	1.995	2.000	2.000	2.000	1.972
Fe^{2+}	0.011	0.000	0.028	0.063	0.000	0.000
Ca	2.959	2.988	2.954	2.933	2.964	3.002

Note: Buffer notation: NNO=NNO-H_2O; CCO=CCO-H_2O; CH4=CCH_4; NaCl=NNO-H_2O-NaCl; HW=Hd + Wo + H_2O; VA = pressure vessel + Ar medium; AH = mixture of Ar and H_2O in pressure vessel.

* Total Fe calculated as FeO from microprobe analysis.

** FeO recalculated as Fe_2O_3 for andradite and as FeO and Fe_2O_3 for magnetite based on charge balance and stoichiometry.

or NaCl with H_2O, Au capsules 30 mm long were used, and the amount of H_2O depended on the temperature and the desired mole fraction of H_2O (X_{H_2O}); 20–30 mg of H_2O were used with 100–180 mg of NaCl, and 10–40 mg of H_2O were used, with appropriate amounts of $Ag_2C_2O_4$, to yield X_{H_2O} of 0.3–0.9. Both the sample assemblage and the H_2 sensor were sealed in Pt tubing of 20 mm × 1.85 mm (od) × 1.54 mm (id). Typically, 30–40 mg of silicates mixed in stoichiometric proportions were used with 10–15 mg H_2O. Sensors contained approximately 20 mg of a Ag-AgCl mixture (in equal amounts by weight), with 10–15 mg H_2O.

After quenching, the presence of H_2O in the buffer assemblage was determined by weighing the Au capsule, puncturing and drying it at 110 °C and then reweighing it. The buffer assemblage was examined optically to ensure the presence of reduced and oxidized phases. For experiments using H_2O-CO_2 mixtures to shift f_{H_2}, the ratio of the fluid components was determined following the technique of Metz (1967). The latter technique was reproducible to ±0.05 mol% CO_2. Sample capsules were cleaned with steel wool, weighed (±0.05 mg), punctured, and dried to determine the gain or loss of H_2O upon oxidation or reduction of the silicate + H_2O assemblage. The sensor capsule was cleaned and then punctured on a Teflon plate with a tungsten carbide needle, and the fluid was collected in microcapillary tubes of 3–10 μL for measurement of M_{Cl^-}.

Calibration of H_2 sensor

The H_2 sensor technique requires calibration against a reference H_2 buffer before it can be applied in a study of this type. Chou (1978, 1987a) discussed in detail the assumptions of the sensor technique and outlined procedures for its calibration and practical application. The pertinent details are summarized here. The calibration of

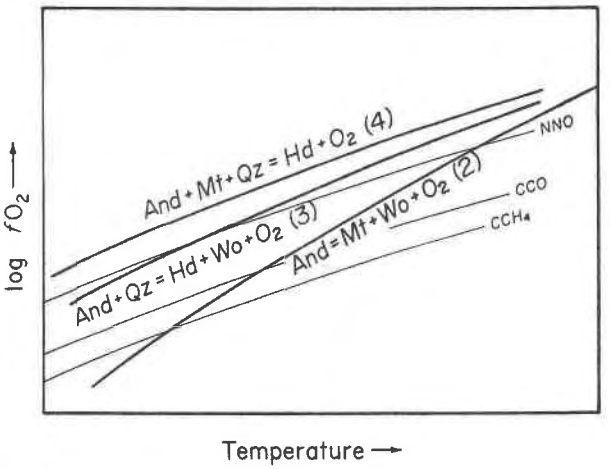

Fig. 3. Positions of the three equilibria investigated relative to O buffers used to generate H_2. Equilibrium 2 intersects NNO, CCO, and CCH_4 at a relatively high angle, allowing reversal of temperature along an O buffer. Equilibrium 3 intersects NNO at a single temperature, and Equilibrium 4 does not intersect NNO in the temperature range investigated for this study. Equilibria 3 and 4 intersect a point on Equilibrium 2 at a high temperature, constraining the relative positions of Equilibria 3 and 4 in f_{O_2}-T space.

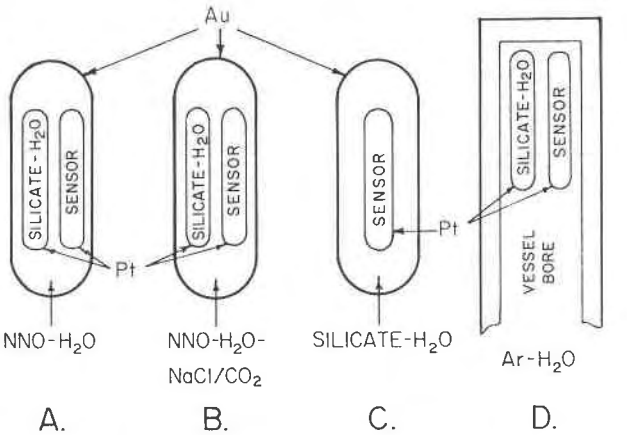

Fig. 4. Experimental configurations used in this study. H_2 sensors were included in all experiments to monitor f_{H_2}. Silicate + H_2O is a mixture of silicates and H_2O for a given equilibrium. **(A)** Conventional configuration (Eugster, 1957), consisting of an O buffer (in this example NNO) and H_2O (H_2 sensor added for this study). **(B)** Conventional configuration with addition of NaCl or CO_2 to allow reduction in f_{H_2O} and f_{H_2}. **(C)** Configuration of Burton et al. (1982) in which an f_{O_2}-dependent silicate reaction serves as source of H_2 by reaction with H_2O, and the intrinsic f_{H_2} of the redox reaction is monitored by a H_2 sensor. **(D)** Silicate sample and sensor placed directly into pressure vessel bore, with f_{H_2} adjusted by varying partial pressures of Ar and H_2O.

the NNO buffer by Huebner and Sato (1970; equation for calculation of f_{O_2} from Huebner, 1971) served as the reference buffer for the H_2 sensors. H_2 sensors containing distilled, deionized H_2O were assembled and loaded in the configuration described above, and then sealed with the NNO-H_2O assemblage in a Au capsule. Duplicate calibration experiments were made in separate vessels at 600 (108 h), 700 (41 h), and 800 °C (12 h) (see initial calibration experiments, Table 3). Chou (1978) has shown that osmotic equilibrium for H_2 diffusion is attained in the respective times at each temperature by reversing the equilibrium m_{HCl} using sensors that started out with pure H_2O and 3 M HCl. The latter correspond to values of m_{HCl} much less than and greater than the equilibrium value, respectively. The final concentrations of m_{HCl} in the two sensors from the bracketing experiments are nearly identical (see also Burton et al., 1982). Therefore, it was deemed adequate to use only one sensor (pure H_2O) in the present calibration and experiments. For the calibration experiments of this study, the measured M_{CL^-} for duplicate experiments at each temperature are reproducible to ± 0.010 M (Table 3).

As stated, the initial H_2 sensor calibration experiments were conducted for periods on the order of 12 to 100 h using the NNO-H_2O assemblage to generate H_2. However, actual experiments required considerably longer times in order to obtain discernible reactions among the silicates (up to 960 h), particularly for experiments on Equilibrium 3 between 600 and 700 °C that were close to the equilibrium boundary. In successively longer experiments buffered at the f_{O_2} of NNO for a given T, the measured M_{Cl^-} increased and asymptotically approached a maximum value (Fig. 5). If the long-term experiments that exhibit the increase in M_{Cl^-} are referenced to short-term experiments, the f_{O_2} calculated for the long-term experiments buffered by NNO-H_2O are erroneously low (0.1 to 0.4 log units below NNO).

To determine if the presence and extent of alloying of Ag from the Ag-AgCl buffer with the Pt capsule wall was the cause of the increase in M_{Cl^-} in the experiments of long duration, sensor capsules from 15 experiments were examined by backscattered electron (BSE) imaging, and wavelength and energy dispersive microprobe analysis. In the calibration and other experiments of short duration, pure Ag metal was present as rounded blebs in a matrix of AgCl. No Pt was detectable in either phase. However, even in the relatively short-term calibration experiments, solid solution of Ag in the Pt capsule wall was evident in BSE images and on EDS spectra of the capsule. There was a compositional gradient from pure Ag at the inner capsule wall to approximately $Ag_{70}Pt_{30}$ over a distance of 50 μm into the capsule. In contrast, the long-term experiments contained no detectable Ag within the AgCl matrix. The compositional gradient in capsules from experiments of long duration was on the order of $Ag_{98}Pt_2$ at the inner wall to approximately $Ag_{70}Pt_{30}$ at the limit of Ag solid solution in the Pt capsule. No Pt was detectable in the AgCl for sensors from long-term experiments. Alloying of Ni with the outer 10 μm of the Pt capsule wall was also detected for the long-term experiments. Between the inner Ag-Pt alloy and outer Ni-Pt alloy the capsule was pure Pt.

The absence of Ag from the Ag-AgCl buffer in experi-

ments of long duration provides an explanation for the increase in M_{Cl^-} in the sensor capsule. The equilibrium constant for Equilibrium 5 is given by Equation 6. If pure Ag is no longer present in the buffer assemblage, the activity of Ag is less than unity. At constant pressure, temperature, f_{H_2}, and activity of AgCl, reduction in the activity of Ag is compensated by an increase in f_{HCl}. This increase in f_{HCl} is reflected in the measured M_{Cl^-} that increases with time (Fig. 5). At 600 °C, no significant change in M_{Cl^-} was found for experiments with durations up to 638 h; the increase of 0.05 M in Cl^- at 960 h corresponds to a decrease of a_{Ag} from 1 to 0.90. Similarly, the observed increase in M_{Cl^-} at 650, 665, and 685 °C corresponds to the decreases of a_{Ag} from 1 down to 0.93, 0.81, and 0.90, respectively.

To compensate for the time dependence of M_{Cl^-}, the following conventions were used to reference experiments:

1. All experiments using pure NNO or CCO are assumed to be buffered at the equilibrium f_{O_2} of the respective system for that experiment, although the sensor may indicate that a particular experiment is at a lower f_{O_2}.

2. Experiments displaced from the NNO buffer for Equilibria 3 and 4 were referenced to the M_{Cl^-} and f_{O_2} for the longest experiment at that temperature (for NNO and pure H_2O). In most cases the reference value was that for sensors for the longest experiment on Equilibrium 3, except experiment HAMS 3a for Equilibrium 4, which was the reference at 800 °C. Reference values for the long-term experiments are given by $\log m_{Cl^-} = 1.565 \times 10^{-3}T(°C) - 1.268$. Experiments at 840 and 860 °C on Equilibrium 3 and at 700 °C on Equilibrium 4 were referenced to an extrapolation of this calibration.

The result of the latter convention is that the calculated f_{O_2} for an experiment displaced from NNO is an upper limit on the best estimate of the equilibrium f_{O_2} for that half reversal. Ideally, one would reference the calculated f_{O_2} of an experiment of any length to a calibration experiment of similar length. This assumes that the difference between the measured M_{Cl^-} for reference and sample remained constant as a function of time. However, we did not obtain information on M_{Cl^-} for all experimental temperatures as a function of time. Rather than making subjective choices for the correct reference value for experiments of intermediate length, the long-term calibration provides a consistent reference for half reversals displaced from NNO. Use of the short-term rather than long-term experiments as a reference results in less than a 0.2-log-unit decrease in f_{O_2} for most experiments.

Thermodynamic calculations

The techniques for calculation and extrapolation of equilibria in P-T-f_{O_2} space used here are summarized in Moecher et al. (1988). Thermodynamic data for andradite, hedenbergite, wollastonite, magnetite, hematite, and quartz, and sources for these data, are also listed therein. The free energies of andradite and hedenbergite are revised in this study.

Results and discussion

Equilibrium 2: 6 And = 4 Mt + 18 Wo + O_2

Reversals for Equilibrium 2 were obtained along the NNO, CCO, and CCH_4 buffers (Fig. 6). Experiments were also made employing the assemblage $WO_2 + H_2O$ as a source of H_2 (Cygan and Chou, 1990), with Ag-AgBr in the H_2 sensors. The assemblage $WO_2 + H_2O$ generates H_2 and $WO_{2.72}$, the buffer being the WO_2-$WO_{2.72}$. Equilibrium 2 was reversed in experiments of 6 to 70 h at 700 to 860 °C.

Microprobe analysis of products from experiments on Equilibrium 2 indicated solid solution of up to 2 at.% Fe in wollastonite [Ca/(Ca + Fe)], approximately a tenfold increase over the starting material (Fig. 2). The most significant impurity in magnetite products was 1–2 at.% Ca [Ca/(Ca + Fe^{2+})]. The change in wollastonite and magnetite compositions may be explained by mutual exchange of Fe and Ca. Andradite exhibited no obvious change in composition relative to the starting material. The unit-cell parameter of andradite from some of the experiments, obtained from powder XRD refinements, is only slightly lower than that of the starting andradite (12.555 Å).

The shift in Equilibrium 2 was calculated taking into account the extent of solid solution in magnetite, wollastonite, and andradite (experiments WAM 21 and WAM 22, 840 and 860 °C). For the most diluted compositions (1.5 at.% Fe in wollastonite, 2 at.% Ca in magnetite, and 1 mol% skiagite component in andradite, and assuming ideal mixing), $\Delta_r G^{2\ kbar}_{m,850\ °C} = 2.5$ kJ·mol^{-1} for each mole of O_2. This corresponds to an isothermal shift in $\log f_{O_2}$ of 0.1 at 850 °C.

Our reversals were used to evaluate the accuracy of two experimental studies on Equilibrium 1. Huckenholz and Yoder (1971) and Suwa et al. (1976) determined the equilibrium temperature at 1 bar of Equilibrium 1 to be 1137 ± 5 °C and 1165 ± 5 °C, respectively. Using these two temperatures as starting points, we calculated the equilibrium temperature for this reaction at 2 kbar using expansivity, compressibility, and entropy data. The addition of Equilibrium 1 and the magnetite-hematite (MH) buffer (calculated from data in Robinson et al., 1982) yields Equilibrium 2. Using the intersection of Equilibrium 1 with MH as a starting point, the position of Equilibrium 2 in f_{O_2}-T space was calculated. The relative positions of Equilibrium 2 for the case of Huckenholz and Yoder's starting point vs. that of Suwa et al. are shown in Figure 6.

The present experimental reversals are most consistent with the experiments of Huckenholz and Yoder. The preferred value of $\Delta_f G^0_{m,298}$ for andradite, calculated from Huckenholz and Yoder's starting point and thermodynamic data in Moecher et al. (1988), is −5428.0 ± 5.9 kJ·mol^{-1}. Using data for the elements from Robie et al. (1979), $\Delta_f H^0_{m,298}$ for andradite is −5770.7 kJ·mol^{-1}.

The quoted uncertainty in $\Delta_f G^0_{m,298}$ for andradite was calculated by simple propagation of errors. The true un-

TABLE 3. Experimental data for Ca-Fe-Si-O-H system at 2-kbar pressure

(a) Equilibrium 2: 6 And = 4 Mt + 18 Wo + O_2

Experiment no.	T (°C)	Buffer	Time (h)	Stable phases	M_{Cl^-} measured	log $m^s_{Cl^-}$	log f_{O_2}	log $m^f_{Cl^-}$	log $f^s_{O_2}$
WAM 1	600	NNO	48	And	0.469(22)	−0.326	−19.09		
WAM 2	700	CCO	47	And	1.464(8)	0.179	−16.17		
WAM 6	750	CCO	28	And	1.640(20)	0.229	−14.92		
WAM 8	775	CCO	20	Wo,Mt	1.944(88)	0.306	−14.34		
WAM 9	760	CCO	20	nr	1.886(19)	0.292	−14.68		
WAM 10	785	CCO	20	Wo,Mt	2.029(60)	0.325	−14.12		
WAM 21	840	NNO	6	And	1.082(10)	0.044	−12.96		
WAM 22	860	NNO	6	Wo, Mt	1.166(31)	0.077	−12.56		
					M_{Br^-} measured	log $m^s_{Br^-}$	log f_{O_2}	log $m^f_{Br^-}$	log $f^s_{O_2}$
WAM 16	685	WO_2-H_2O	20	Wo,Mt	0.294(5)	−0.532	−18.08	−0.931	−19.68(3)
WAM 17	700	WO_2-H_2O	20	Wo,Mt	0.287(23)	−0.543	−17.69	−0.897	−19.10(14)
WAM 18	715	WO_2-H_2O	20	Wo,Mt	0.277(3)	−0.558	−17.31	−0.885	−18.62(2)
WAM 19a	710	CCH_4	48	And	0.201(3)	−0.697	−17.35	−0.904	−18.18(3)
WAM 19b	720	CCH_4	46	And	0.203(10)	−0.693	−17.10	−0.882	−17.86(9)
WAM 20a	750	CCH_4	48	Wo,Mt	0.246(17)	−0.609	−16.39	−0.844	−17.33(12)
WAM 20b	740	CCH_4	46	Wo,Mt	0.206(10)	−0.685	−16.62	−0.856	−17.31(9)

(b) Equilibrium 3: 2 And + 4 Qz = 4 Hd + 2 Wo + O_2

Experiment no.	T (°C)	Buffer	Time (h)	Stable phases	M_{Cl^-} measured	log $m^s_{Cl^-}$	log f_{O_2}	log $m^f_{Cl^-}$	log $f^s_{O_2}$
HAWS 1a+	650	NNO	65	nr	0.567(6)	−0.241	−17.55		
HAWS 1b+	650	NNO	144	nr	0.585(16)	−0.227	−17.55		
HAWS 1c+	650	NNO	408	Hd,Wo	0.601(25)	−0.216	−17.55		
HAWS 1d	650	NNO	673	nr	0.607(19)	−0.211	−17.55		
HAWS 1e	650	NNO-NaCl	276	And,Qz(Hd,Wo)	0.503(48)	−0.294	−17.55	−0.211	−17.22(17)
HAWS 2a+	665	NNO	65	nr	0.558(2)	−0.248	−17.12		
HAWS 2b+	665	NNO	144	nr	0.589(16)	−0.224	−17.12		
HAWS 2c	665	NNO	408	Hd,Wo(And,Qz)	0.673(6)	−0.166	−17.12		
HAWS 2d	665	NNO	673	Hd,Wo(And,Qz)	0.691(18)	−0.154	−17.12		
HAWS 2e	665	NNO-NaCL	384	And,Qz(Hd,Wo)	0.451(19)	−0.341	−17.12	−0.189	−16.51(7)
HAWS 2f	665	NNO	497	Hd,Wo(And,Qz)	0.668(26)	−0.169	−17.12		
HAWS 3a+	685	NNO	65	nr	0.622(12)	−0.200	−16.57		
HAWS 3b+	685	NNO	144	nr	0.663(28)	−0.172	−16.57		
HAWS 3d	685	NNO	641	Hd,Wo(And,Qz)	0.692(10)	−0.154	−16.57		
HAWS 3e	685	NNO-NaCl	384	And,Qz(Hd,Wo)	0.453(8)	−0.340	−16.57	−0.154	−15.83(4)
HAWS 4a	700	NNO	65	Hd,Wo	0.659(6)	−0.175	−16.17		
HAWS 4b	700	NNO-NaCl	74	And,Qz(Hd,Wo)	0.433(4)	−0.359	−16.17	−0.172	−15.42(1)
HAWS 4c	700	NNO-CO_2	114	nr	0.512(13)	−0.286	−16.17	−0.172	−15.71(4)
HAWS 4d	700	Vessel-H_2O	167	And,Qz(Hd,Wo)	0.280(8)	−0.550	−16.17	−0.172	−14.66(5)
HAWS 6a+	640	NNO	72	nr	0.546(13)	−0.263	−17.85		
HAWS 7a+	800	HAWS	6	And,Qz	0.328(10)	−0.481	−13.79	0.015	−11.80(5)
HAWS 7b-2	800	HW	10.5	Hd,Wo	0.693(15)	−0.153	−13.79	0.015	−13.12(4)
HAWS 7b-3	800	HW	18	And	0.429(9)	−0.363	−13.79	0.015	−12.28(4)
HAWS 8a+	800	NNO-CO_2	17.5	Hd,Wo	0.859(14)	−0.058	−13.79	0.015	−13.50(3)
HAWS 8b+	800	NNO-CO_2	12.5	Hd,Wo	0.689(15)	−0.155	−13.79	0.015	−13.11(4)
HAWS 8c	800	NNO-CO_2	26	Hd,Wo	0.766(16))	−0.109	−13.79	0.015	−13.29(3)
HAWS 8d	800	NNO-CO_2	19	Hd,Wo	0.572(8)	−0.237	−13.79	0.015	−12.78(2)
HAWS 9a+	600	NNO	124	nr	0.444(4)	−0.348	−19.09		
HAWS 9c	600	HAWS	283	And(Hd,Wo)	0.220(6)	−0.655	−19.09	−0.295	−17.65(5)
HAWS 9c-3	600	NNO	638	And,Qz,Wo(Hd)	0.451(5)	−0.341	−19.09		
HAWS 9d	600	NNO	960	And,Qz(Hd,Wo)	0.501(15)	−0.295	−19.09		
HAWS 9e	600	NNO-NaCl	812	And,Qz(Hd,Wo)	0.391(17)	−0.404	−19.09	−0.295	−18.66(8)
HAWS 10b+	600	CCO	283	Hd,Wo(And,Qz)	0.952(82)	−0.013	−20.56		
HAWS 10c	600	CCO-NaCL	276	Hd,Wo(And,Qz)	0.709(44)	−0.143	−20.56	−0.024	−20.08(11)
HAWS 11a	625	NNO	673	nr	0.560(21)	−0.247	−18.30		
HAWS 11b	625	NNO-NaCl	573	And,Qz(Hd,Wo)	0.407(22)	−0.386	−18.30	−0.247	−17.74(9)
HAWS 12a	750	NNO	74	Hd,Wo	0.866(68)	−0.055	−14.92		
HAWS 12b	750	NNO-CO_2	53	And,Qz(Hd,Wo)	0.451(15)	−0.341	−14.92	−0.055	−13.77(5)
HAWS 12c	750	NNO-CO_2	53	nr	0.569(15)	−0.240	−14.92	−0.055	−14.18(5)
HAWS 12d	750	NNO-NaCl	70	And,Qz(Hd,Wo)	0.484(3)	−0.311	−14.92	−0.055	−13.90(2)

(c) Equilibrium 4: 3 And + Mt + 9 Qz = 9 Hd + 2 O_2

Experiment no.	T (°C)	Buffer	Time (h)	Stable phases	M_{Cl^-} measured	log $m^s_{Cl^-}$	log f_{O_2}	log $m^f_{Cl^-}$	log $f^s_{O_2}$
HAMS 1a+	600	NNO	94	Qz,And(Wo)	0.463(4)	−0.330	−19.09		
HAMS 1b+	600	NNO	94	Qz,And(Wo)	0.436(7)	−0.356	−19.09		

TABLE 3.—*Continued*

Experiment no.	T (°C)	Buffer	Time (h)	Stable phases	M_{Cl^-} measured	log $m^s_{Cl^-}$	log f_{O_2}	log $m^r_{Cl^-}$	log $f^s_{O_2}$
HAMS 3a+	800	NNO	20	Hd,Wo	1.013(1)	0.015	−13.79		
HAMS 3b+	800	NNO-CO_2	20	Hd,Wo	0.957(35)	−0.010	−13.79	0.015	−13.69(6)
HAMS 3c+	800	NNO-CO_2	20	Hd	0.515(3)	−0.283	−13.79	0.015	−12.60(1)
HAMS 3d+	800	NNO-CO_2	20	Hd	0.703(3)	−0.147	−13.79	0.015	−13.14(1)
HAMS 4a+	600	NNO	283	Hd	0.454(13)	−0.339	−19.09		
HAMS 4b	600	NNO-NaCl	362	Hd(And,Qz)	0.399(9)	−0.395	−19.09	−0.295	−18.69(4)
HAMS 5a+	600	Vessel-Ar	252	And,Mt,Qz	0.027(11)	−1.561	−19.09	−0.295	−14.03(89)
HAMS 5b	600	Vessel-Ar	276	And,Mt,Qz(Hd)	0.144(10)	−0.839	−19.09	−0.295	−16.92(13)
HAMS 6a+	650	NNO	135	Hd(And,Mt,Qz)	0.566(3)	−0.242	−17.55		
HAMS 6b+	650	Vessel-Ar	135	And,Mt,Qz(Hd)	0.240(2)	−0.617	−17.55	−0.211	−15.93(2)
HAMS 6c	650	Vessel-H_2O	285	Hd,Wo(Mt)	0.794(16)	−0.093	−17.55	−0.211	−18.02(3)
HAMS 6d	650	Ar-H_2O	242	nr	0.365(8)	−0.434	−17.55	−0.211	−16.66(4)
HAMS 6e	650	Ar-H_2O	330	And,Mt,Qz(Hd)	0.150(14)	−0.821	−17.55	−0.211	−15.11(17)
HAMS 6f	650	NNO-NaCl	623	And,Qz(Hd)	0.467(19)	−0.326	−17.77	−0.211	−17.09(7)
HAMS 6g	650	Ar-H_2O	184	And,Mt,Qz(Hd)	0.123(6)	−0.908	−17.55	−0.211	−14.76(8)
HAMS 7a+	700	Vessel-Ar	132	And,Mt,Qz	0.222(4)	−0.651	−16.17	−0.135	−14.10(3)
HAMS 7b	700	Vessel-H_2O	167	And,Qz,Mt(Hd)	0.280(8)	−0.550	−16.17	−0.135	−14.50(4)
HAMS 7c-2	700	NNO-NaCl	242	And,Qz(Hd)	0.531(15)	−0.270	−16.17	−0.135	−15.63(5)
HAMS 7c-3	700	NNO-NaCl	190	And,Qz(Hd)	0.475(15)	−0.319	−16.17	−0.135	−15.43(5)
HAMS 7d	700	Ar-H_2O	48	Hd grew (Wo)	0.678(7)	−0.163	−16.17	−0.135	−16.06(2)
HAMS 7e	700	Ar-H_2O	168	And,Qz(Hd,Wo)	0.337(13)	−0.469	−16.17	−0.135	−14.83(3)
HAMS 7f	700	Ar-H_2O	191	And,Qz(Hd)	0.358(12)	−0.442	−16.17	−0.135	−14.94(6)
HAMS 8a+	750	Vessel-Ar	65	And,Mt,Qz	0.216(5)	−0.663	−14.92	−0.055	−12.49(4)
HAMS 8b	750	NNO-NaCl	117	And,Mt,Qz(Hd)	0.457(13)	−0.336	−14.92	−0.055	−13.80(5)

Initial H_2 sensor calibration experiments on NNO-H_2O buffer

Experiment no.	T (°C)	Time (h)	M_{Cl^-} measured	log $m^s_{Cl^-}$	log f_{O_2}
TEST 1	700	41	0.669(3)	−0.167	−16.167
TEST 2	700	41	0.677(10)	−0.163	−16.167
TEST 5	800	12	0.944(14)	−0.017	−13.788
TEST 6	800	12	0.936(9)	−0.020	−13.788
TEST 7	600	108	0.471(10)	−0.322	−19.091
TEST 8	600	108	0.452(9)	−0.341	−19.091

Note: All WAM experiments and experiments denoted by + used andradite I; all others used andradite II. Labels r and *s*: values of molality (*m*) of measured Cl^- or Br^- concentration, and f_{O_2} for reference buffer and sample, respectively. Reference values of M_{Cl^-} for CCO and CCH_4 are from Chou (1978, 1987b). Values in parentheses are 1σ standard deviations of average of 2–4 analyses of M_{Cl^-}, and calculated uncertainties in $f^s_{O_2}$ resulting from chloride precision. NNO reference buffer values were calculated from $\log f_{O_2} = 9.36 - 24930/T + 0.046(P - 1)/T$ (Huebner, 1971). Buffer notation as in Table 2. Abbreviations: nr: no reaction; ( ) trace phase; And: andradite; Hd: hedenbergite; Mt: magnetite; Qz: quartz; Wo: wollastonite. WAM = (W)ollastonite + (A)ndradite + (M)agnetite; HAWS = (H)edenbergite + (A)ndradite + (W)ollastonite + (S)ilica (Quartz); HAMS = (H)edenbergite + (A)ndradite + (M)agnetite + (S)ilica (Quartz). HAWS experiments 4c and 8a–8d had $X_{CO_2} = 0.50$, 0.77, 0.47, 0.50, and 0.30, respectively. HAMS experiments 3b–3d had $X_{CO_2} = 0.12$, 0.72, and 0.67, respectively.

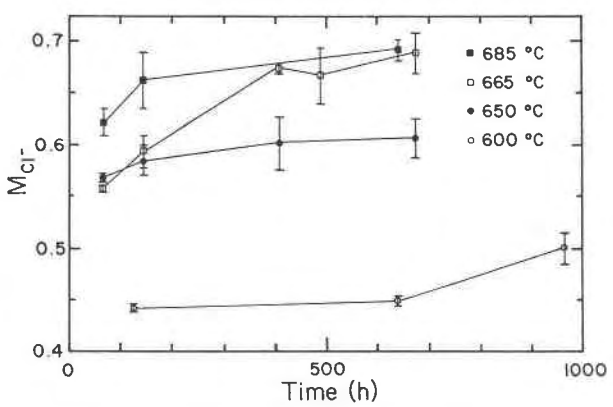

Fig. 5. Measured M_{Cl^-} from H_2 sensor in samples at four temperatures, showing variations as a function of time. H_2 was generated by NNO-H_2O in Au capsules. The long-term increase in M_{Cl^-} reflects solid solution of Ag from the Ag-AgCl buffer with the Pt capsule wall, and decrease in activity of Ag.

certainty is likely much less than this value. Our reversals for Equilibrium 2 allow us to distinguish between the two studies on Equilibrium 1. If the reversal of Suwa et al. (1976) for Equilibrium 1 is used as the starting point for the calculation of $\Delta_f G^0_{m,298}$ (And), we obtain −5429.2 kJ·mol^{-1}, which is only 1.2 kJ more negative than the value calculated above.

The reversals of Gustafson (1974) on Equilibrium 2 at 0.5, 1.0, and 2.0 kbar, along with the calculated position of Equilibrium 2 based on Huckenholz and Yoder's data, are shown in Figure 6. Our reversals on NNO lie at slightly higher temperature than Gustafson's. A systematic shift to lower temperature is present in the location of Gustafson's reversals relative to the calculated location of Equilibrium 2 based on the results of both Huckenholz and Yoder (1971) and Suwa et al. (1976). However, considering a ±5 °C uncertainty in reported temperatures, Gustafson's reversals at 0.5 and 1 kbar are consistent with the calculated position of Equilibrium 2, and the present reversals.

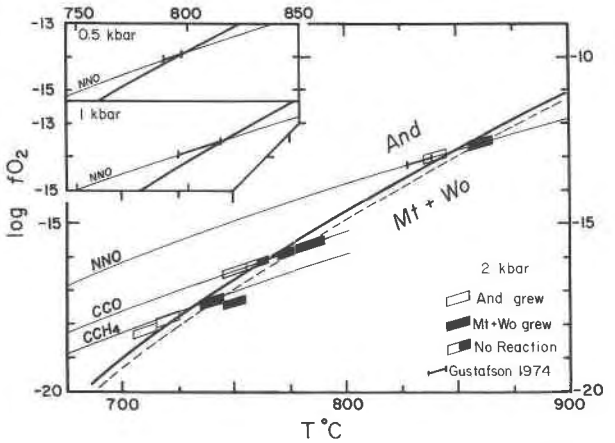

Fig. 6. Experimental reversals for Equilibrium 2. Heavy line is the position of Equilibrium 2 calculated from the intersection of Equilibrium 1 (And = Hm + 3 Wo; reversal of Huckenholz and Yoder, 1971) with the magnetite-hematite buffer; dashed line is the calculated position of Equilibrium 2 based on the reversal of Suwa et al. (1976) for Equilibrium 1. Also shown are the reversals for Equilibrium 2 of Gustafson (1974) at 0.5, 1.0 (inset), and 2-kbar pressure on NNO.

A lower limit on the stability of andradite as a function of f_{O_2} was constrained by experiments using the WO_2-$WO_{2.72}$ buffer. At 700 ± 15 °C and $\log f_{O_2} = -19.0 \pm 0.5$, andradite reacted to kirschsteinite and magnetite. This is 2 log units more oxidizing than the half reversal of Gustafson for the same reaction on the wüstite-magnetite buffer.

Equilibrium 3: 2 And + 4 Qz = 4 Hd + 2 Wo + O_2

Reversals for Equilibrium 3 (Fig. 7) required experiments of 6 to 960 h (Table 3). Longer experiments were necessary as the equilibrium boundary was approached. Shorter experiments at a given f_{O_2} and T that indicated no reaction were conducted again for successively longer periods. Reversals were obtained along NNO by using configuration A (Fig. 4) and at constant temperature by using configurations B and C (Fig. 4).

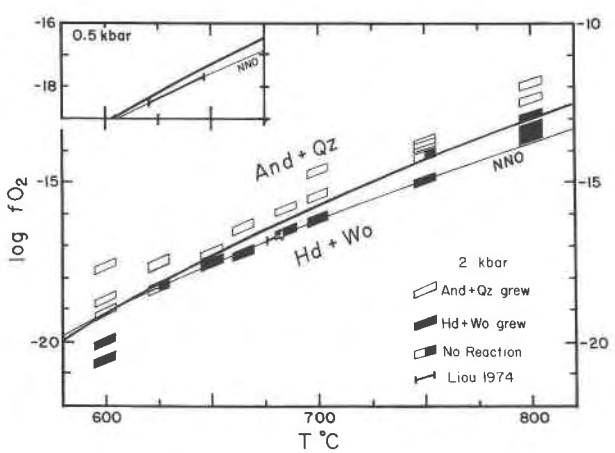

Fig. 7. Experimental reversals for Equilibrium 3. Heavy line is the position of Equilibrium 3 calculated using reversal at 650 °C and $\log f_{O_2} = -17.35$ as a starting point. Inset shows reversals of Liou (1974) at 2- and 0.5-kbar pressure on NNO.

The reversal at $\log f_{O_2} = -17.35$, $T = 650$ °C, was used as a starting point for calculation of the position of Equilibrium 3 (Fig. 7). The calculated result is consistent with most of the reversals. The experiments at 800 °C that indicate growth of hedenbergite + wollastonite most likely are upper f_{O_2} limits (lower limits on f_{H_2}) for those experiments for two reasons. First, as discussed previously, referencing f_{O_2} to experiments of long duration will result in upper limits on f_{O_2} for shorter experiments. Second, experiments at 800 °C that indicate growth of hedenbergite + wollastonite employed mixtures of NNO + H_2O + CO_2. As H_2O decomposes and H_2 diffusion occurs, the mole fraction and fugacity of H_2O in the fluid phase continuously decreases, and the mole fraction of CO_2 increases. The rate of diffusion of H_2 out of the Au capsule is much greater at 800 °C than at lower temperatures. The H_2 sensor should continuously equilibrate with the changing f_{H_2} and should therefore record the f_{H_2} at the end of the experiment. However, the silicate assemblage may have equilibrated early in the experiment at slightly higher f_{H_2O} and f_{H_2}. Therefore, these f_{O_2} values are considered upper limits for Equilibrium 3 at 800 °C.

Microprobe analysis of products from experiments on Equilibrium 3 indicated that the extent of solid solution is 1–2% for all phases (Table 2). Solid solution of this amount results in a shift in f_{O_2} for Equilibrium 3 of less than 0.1 log units.

The reversal at 650 °C was also used to calculate the free energy of hedenbergite by first calculating the free energy of Equilibrium 3 at 1 bar, 25 °C. Using the free energy of andradite calculated above, $\Delta_f G^0_{m,298}$ for hedenbergite is -2676.6 ± 5.3 kJ·mol^{-1}. Using thermodynamic data for the elements from Robie et al. (1979), $\Delta_f H^0_{m,298}$ for hedenbergite is -2840.4 kJ·mol^{-1}.

Equilibrium 4: 3 And + Mt + 9 Qz = 9 Hd + 2 O_2

Experiments on Equilibrium 4 (Table 3) were made from 600 to 800 °C using configurations B, C, and D (Fig. 4; reversals shown in Fig. 8). Most experiments exhibited unequivocal indications of reaction direction. However, because of the proximity of Equilibria 3 and 4 in f_{O_2}-T space, hedenbergite is stable with andradite and quartz over a limited range in f_{O_2} (Figs. 3 and 8). Many experiments to bracket Equilibrium 4 that were in the f_{O_2}-T region between Equilibria 3 and 4 indicated loss of magnetite and growth of andradite and quartz. This occurrence was taken to indicate that the boundary for Equilibrium 4 had been overstepped, but not enough to result in formation of wollastonite by Equilibrium 3.

Microprobe analysis of hedenbergite experiment products indicated a deficiency in Ca relative to Fe of about 1%. Andradite indicated no discernible systematic difference in composition from the starting material. The effect of these solid solutions on displacement of the equilibrium boundary is less than 0.1 log unit in f_{O_2}.

The location of Equilibrium 4 is constrained by the

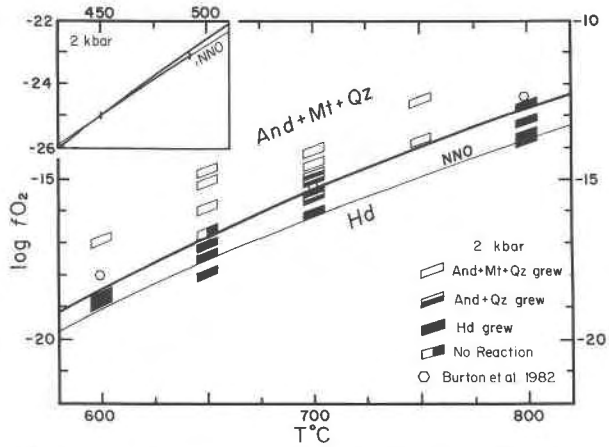

Fig. 8. Experimental reversals for Equilibrium 4. Heavy line is the position of Equilibrium 4 calculated using intersection of Equilibria 2 and 3 as a starting point. Also shown are results of Burton et al. (1982) (hexagons) and Gustafson (1974) (inset, bars), both at 2-kbar pressure.

locus of the intersection of Equilibria 2 and 3. By using this intersection as a starting point (931 °C, log f_{O_2} = −10.1), the position of Equilibrium 4 was calculated at lower temperature (Fig. 8). The reversals agree reasonably well, except for the bracket at 800 °C, which is slightly higher than the calculated position. This may be ascribed to the same processes invoked above for similar capsule configurations used on Equilibrium 3.

The calculated position of Equilibrium 4 relative to the 2-kbar reversal of Gustafson (1974) is shown in the insert of Figure 8. Equilibrium 4 intersects the low-temperature end of Gustafson's reversal. If the position of Equilibrium 4 is constrained to fit the reversal of Gustafson, the f_{O_2} value must be shifted −0.1 log unit. Because of the constraint on the position of Equilibria 3 and 4 imposed by their intersection with Equilibrium 2 (Fig. 4), the position of Equilibrium 3 must also shift to lower f_{O_2}. This shift in Equilibrium 3 is in the correct direction but is not of sufficient magnitude to fit the reversal of Liou (1974) at 2 kbar (Fig. 7).

The experimental results of Burton et al. (1982) on Equilibrium 4, although in reasonable agreement with our reversals, lie at slightly higher f_{O_2} than the calculated position (Fig. 8). This may be caused by the experimental configuration used in the former study, which consisted of the silicate assemblage in stoichiometric proportions enclosing a H_2 sensor (Fig. 4C). The assemblage hedenbergite + andradite + magnetite + quartz generates H_2 by reduction of H_2O, in the same manner as an O buffer. Generation of a steady-state f_{H_2} is relatively sluggish for silicate redox equilibria (e.g., fayalite-magnetite-quartz: Chou and Cygan, 1990), and quenching of the experiment and analysis of the sensor before this steady state is reached may yield underestimates of the equilibrium f_{H_2} and overestimates of f_{O_2} (or an upper constraint on f_{O_2}). This is likely the case for the experiments of Burton et al. (1982), particularly for the experiments at 600 °C in which reaction among the silicates is likely to be much slower and for which experimental times were much shorter than the present study. We used the same approach as Burton et al. (1982) for Equilibrium 3, except that mixtures of hedenbergite + wollastonite seeded with approximately 5% andradite + quartz were used. The extra mass of hedenbergite + wollastonite permits a greater degree of reaction to occur (and thus more H_2 to be generated), facilitating the approach to equilibrium.

TABLE 4. Comparison of $\Delta_f G^\circ_{m,298}$ for andradite and hedenbergite from various studies (kJ·mol^{-1})

Study	Andradite	Hedenbergite
Helgeson et al. (1978)	−5428.7	−2674.5
Taylor & Liou (1978)	−5411.8	ne
Robie et al. (1987)	−5414.8*	−2674.3
Moecher et al. (1988)	−5424.8**	−2677.7
Kiseleva et al. (1989)	−5405.7†	ne
This study	−5428.0	−2676.6

Note: The abbreviation ne = not evaluated.

* Value quoted by Robie et al. (1987) is an error. Correct value is −5426.0 kJ·mol (R.A. Robie, personal communication, 1989).

** Value given in Table 1 of Moecher et al. (1988), −5413.2, is an error. Correct value is given here.

† The $\Delta_f G^\circ_{m,298}$ calculated from $\Delta_f H^\circ_{m,298}$ = −5748.4, determined calorimetrically by Kiseleva et al. (1989), using data from elements of Robie et al. (1979).

Summary

The experimental results provide reasonably precise and consistent constraints on the position of four andradite and hedenbergite equilibria. The present results agree with those of Huckenholz and Yoder (1971) on Equilibrium 1 and Gustafson (1974) on Equilibrium 2. Aside from the new experimental data presented here, this study illustrates the utility of the H_2 sensor technique in studying redox equilibria (also see Chou and Cygan, 1990). H_2 sensors provide access to a wide f_{O_2}-T range, and experimental studies on redox equilibria need not be confined to f_{O_2}-T conditions along a univariant O buffer. The H_2 sensors need only be referenced to an O buffer close to the f_{O_2} conditions one wishes to study.

The free energies of andradite and hedenbergite determined from these new experimental data were calculated relative to thermodynamic data for hematite, wollastonite, magnetite, and quartz contained in the internally consistent data set of Moecher et al. (1988). These free energies may be compared to values determined in previous studies listed in Table 4. However, our experimental results may be incorporated into other internally consistent thermodynamic data sets (e.g., Berman, 1988; Holland and Powell, 1990), and yield free energies that are slightly different from those calculated here.

The primary motivation for this study was to obtain more accurate estimates of the free energy of hedenbergite and to more accurately constrain the location of a geobarometer based on the Equilibrium 3 hedenbergite + 3 anorthite = 2 grossular + almandine + 3 quartz (Moecher et al., 1988). The value of the free energy of hedenbergite calculated from the new experimental data is 1.1 kJ·mol more negative than that calculated by Moecher et al. (1988). This difference shifts the locus of

the end-member reaction (and, on average, calculated pressures) by −0.6 kbar. The previous calibration of the geobarometer tended to overestimate pressure relative to that obtained by orthopyroxene-garnet-plagioclase-quartz geobarometers and constraints imposed by the kyanite-sillimanite transition. The revised free energy of hedenbergite yields an improved calibration for the hedenbergite-anorthite-grossular-almandine-quartz geobarometer that is now more consistent with other petrologic constraints.

Acknowledgments

This study was carried out at the U.S. Geological Survey, Reston, Virginia, under the auspices of the National Research Council associateship program. We thank G.L. Cygan, H.T. Haselton, and J.S. Huebner for advice during the course of this study and for access to their experimental equipment and laboratories. The comments of Paul Barton and R.A. Robie were helpful in revising early drafts of the manuscript. Formal reviews by J.G. Liou and R.W. Luth significantly improved our presentation of the results.

References cited

Albee, A.L., and Ray, L. (1970) Correction factors for electron probe microanalysis of silicates, oxides, carbonates, phosphates, and sulfates. Analytical Chemistry, 42, 1408–1414.

Bence, A.E., and Albee, A.L. (1968) Empirical correction factors for the electron microanalysis of silicates and oxides. Journal of Petrology, 76, 382–403.

Berman, R.G. (1988) Internally-consistent thermodynamic data for minerals in the system Na_2O-K_2O-CaO-MgO-FeO-Fe_2O_3-Al_2O_3-SiO_2-TiO_2-H_2O-CO_2. Journal of Petrology, 29, 445–522.

Buerger, M.J., and Prewitt, C.T. (1961) The crystal structures of wollastonite and pectolite. Proceedings of the National Academy of Science, 47, 1884–1888.

Burton, J.C., Taylor, L.A., and Chou, I-Ming (1982) The f_{O_2}-T and f_{S_2}-T stability relations of hedenbergite and of hedenbergite-johannsenite solid solutions. Economic Geology, 77, 764–783.

Cameron, M., Sueno, S., Prewitt, C.T., and Papike, J.J. (1973) High temperature crystal chemistry of acmite, diopside, hedenbergite, jadeite, spodumene, and ureyite. American Mineralogist, 58, 594–618.

Chou, I-Ming (1978) Calibration of oxygen buffers at elevated P and T using the hydrogen fugacity sensor. American Mineralogist, 63, 690–703.

——— (1987a) Oxygen buffer and hydrogen sensor techniques at elevated pressures and temperatures. In G.C. Ulmer and H.L. Barnes, Eds., Hydrothermal experimental techniques, p. 61–99. Wiley-Interscience, New York.

——— (1987b) Calibration of the graphite-methane buffer using f_{H_2} sensors at 2 kilobar pressure. American Mineralogist, 72, 76–81.

——— (1988) Quantitative redox control in hydrothermal experiments. Eos, 69, 528.

Chou, I-Ming, and Cygan, G.L. (1990) Quantitative redox control and measurement in hydrothermal experiments. In R.J. Spencer and I-Ming Chou, Eds., The Geochemical Society Special Publication Number 2, 3–15.

Chou, I-Ming, and Eugster, H.P. (1976) A sensor for hydrogen fugacities at elevated pressure and temperature and applications. Eos, 57, 340.

Cygan, G.L., and Chou, I-Ming (1990) The assemblage WO_2 + H_2O as a steady-state hydrogen source in moderately reduced hydrothermal experiments. American Mineralogist, 75, 1399–1405.

Einaudi, M.T., Meinert, L.D., and Newberry, R.J. (1981) Skarn deposits. Economic Geology 75th Anniversary Volume, 317–391.

Ellis, D.J., and Green, D.H. (1979) An experimental study of the effect of Ca upon garnet-clinopyroxene Fe-Mg exchange equilibria. Contributions to Mineralogy and Petrology, 71, 13–22.

Eugster, H.P. (1957) Heterogeneous reactions involving oxidation and reduction at high pressures and temperatures. Journal of Chemical Physics, 26, 1760–1761.

Frantz, J.D., and Eugster, H.P. (1973) Acid-base buffers: Use of Ag + AgCl in the experimental control of solution equilibria at elevated pressures and temperatures. American Journal of Science, 273, 268–286.

Frantz, J.D., and Marshall, W.L. (1984) Electrical conductances and ionization constants of salts, acids, and bases in supercritical aqueous fluids: I. Hydrochloric acid from 100 to 700 °C and at pressures to 4000 bars. American Journal of Science, 284, 651–667.

Gunter, W.D., Chou, I-Ming, and Girsperger, S. (1983) Phase relations in the system NaCl-KCl-H_2O: II. Differential thermal analysis of the halite liquidus in the NaCl-H_2O binary above 450 °C. Geochimica et Cosmochimica Acta, 47, 863–873.

Gustafson, W.I. (1974) The stability of andradite, hedenbergite, and related minerals in the system Ca-Fe-Si-O-H. Journal of Petrology, 15, 455–496.

Haselton, H.T. Jr., Robie, R.A., and Hemingway, B.S. (1987) Heat capacities of synthetic hedenbergite, ferrobustamite, and $CaFeSi_2O_6$ glass. Geochimica et Cosmochimica Acta, 51, 2211–2217.

Helgeson, H.C., Delany, J.M., Nesbitt, H.W., and Bird, D.K. (1978) Summary and critique of the thermodynamic properties of rock-forming minerals. American Journal of Science, 278-A, 229 p.

Holland, T.J.B., and Powell, R. (1990) An enlarged and updated internally consistent thermodynamic dataset with uncertainties and correlations: The system K_2O-Na_2O-CaO-MgO-MnO-FeO-Fe_2O_3-Al_2O_3-TiO_2-SiO_2-CO_2-H_2-O. Journal of Metamorphic Petrology, 8, 89–124.

Huckenholz, H.G., and Fehr, K.T. (1982) Stability relationships of grossular + quartz + wollastonite + anorthite. II. The effect of grandite-hydrograndite solid solution. Neues Jahrbuch für Mineralogie Abhandlungen, 145, 1–33.

Huckenholz, H.G., and Yoder, H.S., Jr. (1971) Andradite stability relations in the $CaSiO_3$-Fe_2O_3 join up to 30 Kb. Neues Jahrbuch für Mineralogie Abhandlungen, 114, 246–280.

Huebner, J.S. (1971) Buffering techniques for hydrostatic systems at elevated pressures. In G.C. Ulmer, Ed., Research techniques for high pressure and high temperatures, p. 123–177. Springer-Verlag, New York.

Huebner, J.S., and Papike, J.J. (1970) Synthesis and crystal chemistry of sodium-potassium richterite $(Na,K)NaCaMg_5Si_8O_{22}(OH,F)_2$: A model for amphiboles. American Mineralogist, 55, 1973–1992.

Huebner, J.S., and Sato, M. (1970) The oxygen fugacity-temperature relationships of manganese and nickel oxide buffers. American Mineralogist, 55, 934–952.

Kandelin, J., and Weidner, D.J. (1988) Elastic properties of hedenbergite. Journal of Geophysical Research, 93, 1063–1072.

Kiseleva, I.A., Ogorodova, L.P., and Sokolova, E.L. (1989) Enthalpy of formation of andradite. Geokhimiya, 1989, 125–131.

Krupka, K.M., Robie, R.A., Hemingway, B.S., Kerrick, D.M., and Ito, J. (1985) Low-temperature heat capacities and derived thermodynamic properties of anthophyllite, diopside, enstatite, bronzite, and wollastonite. American Mineralogist, 70, 249–260.

Lindsley, D.H. (1967) The join hedenbergite-ferrosilite at high pressures and temperatures. Carnegie Institution of Washington Year Book, 65, 230–234.

Liou, J.G. (1974) Stability relations of andradite-quartz in the system Ca-Fe-Si-O-H. American Mineralogist, 59, 1016–1025.

Luth, R.W., Virgo, D., Boyd, F.R., and Wood, B.J. (1989) Ferric iron in mantle-derived garnets. Implications for thermobarometry and for the oxidation state of the mantle. Contributions to Mineralogy and Petrology, 104, 56–72.

Matsueda, H. (1973) Iron-wollastonite from the Sampo mine showing properties distinct from those of wollastonite. Mineralogical Journal, 7, 180–201.

Meinert, L.D. (1982) Skarn, manto, and breccia pipe formation in sedimentary rocks of the Cananea Mining District, Sonora, Mexico. Economic Geology, 77, 919–949.

Metz, P. (1967) Experimentelle Bildung von Forsterit und Calcit aus Tremolite und Dolomit. Geochimica et Cosmochimica Acta, 31, 1517–1532.

Moecher, D.P., Essene, E.J., and Anovitz, L.M. (1988) Calculation of clinopyroxene-garnet-plagioclase-quartz geobarometers and applica-

tion to high grade metamorphic rocks. Contributions to Mineralogy and Petrology, 100, 92–106.

Pattison, D., and Newton, R.C. (1989) Reversed experimental calibration of the garnet-clinopyroxene Fe-Mg exchange thermometer. Contributions to Mineralogy and Petrology, 101, 87–103.

Popp, R.K., Nagy, K.L., and Hajash, A., Jr. (1984) Semiquantitative control of hydrogen fugacity in rapid-quench hydrothermal vessels. American Mineralogist, 69, 557–562.

Robie, R.A., Hemingway, B.S., and Fisher, J.R. (1979) Thermodynamic properties of minerals and related substances at 298.15 K and 1 bar (10^5 pascals) pressure and at higher temperatures. U.S. Geological Survey Bulletin 1452, 456 p.

Robie, R.A., Zhao, B., Hemingway, B.S., and Barton, M.D. (1987) Heat capacity and thermodynamic properties of andradite garnet, $Ca_3Fe_2Si_3O_{12}$, between 10 and 1000 K and revised values of $\Delta_f G^0_{m,298}$ of hedenbergite and wollastonite. Geochimica et Cosmochimica Acta, 51, 2219–2224.

Robinson, G.R., Jr., Haas, J.L., Jr., Schafer, C.M., and Haselton, H.T., Jr. (1982) Thermodynamic and thermophysical properties of selected phases in the MgO-SiO_2-H_2O-CO_2, CaO-Al_2O_3-SiO_2-H_2O-CO_2, and FeO-Fe_2O_3-SiO_2 chemical systems, with special emphasis on the properties of basalts and their mineral components. U.S. Geological Survey Open File Report 83-79, 429 p.

Rutstein, M.S. (1971) Re-examination of the wollastonite-hedenbergite ($CaSiO_3$-$CaFeSi_2O_6$) equilibria. American Mineralogist, 56, 2040–2052.

Shaw, H.R. (1963) Hydrogen-water vapor mixtures; control of hydrothermal atmospheres by hydrogen osmosis. Science, 139, 1220–1222.

——— (1967) Hydrogen osmosis in hydrothermal experiments. In P.H. Abelson, Ed., Researches in geochemistry, vol. 2, p. 521–541. Wiley, New York.

Suwa, Y., Tami, Y., and Naka, S. (1976) Stability of synthetic andradite at atmospheric pressure. American Mineralogist, 61, 26–28.

Taylor, B.E., and Liou, J.G. (1978) The low-temperature stability of andradite in C-O-H fluids. American Mineralogist, 63, 378–393.

Veblen, D.R., and Burnham, C.W. (1970) The crystal structure of hedenbergite and ferrosilite. Canadian Mineralogist, 10, 147.

Whitney, J.A. (1972) The effect of reduced H_2O fugacity on the buffering of oxygen fugacity in hydrothermal experiments. American Mineralogist, 57, 1902–1908.

Wones, D.R. (1989) Significance of the assemblage titanite + magnetite + quartz in granitic rocks. American Mineralogist, 74, 744–749.

Manuscript received December 5, 1989
Manuscript accepted September 20, 1990